Determination of intrinsic magnetic properties of hard magnetic materials from demagnetization curves of polycrystalline samples

S. Wirth, MARTECH, Florida State University, Tallahassee, FL 32306-4351, USA

Abstract

Fitting of demagnetization curves (DMC) can be used for simultaneous determination of anisotropy constants, saturation polarization and texture parameters of polycrystalline hard magnetic materials. Therein, the reversible rotational magnetization processes determining the DMC in the first quadrant of the *J*-*H*-plane after initial saturation of the sample are analyzed. The basic procedure for DMC fitting takes into account anisotropy constants K_1 and K_2 of magnetically uniaxial compounds and a parameter describing a rotationally symmetric texture. In case of $Sm_2Fe_{17}Z_x$ (Z = N, C, H), the results on K_1 and K_2 are further analyzed to determine the crystal–field parameters. The basic procedure can be extended to investigate more complex materials. As examples, a non-uniaxial type of magnetocrystalline anisotropy and different types of texture which are of practical interest are discussed. Furthermore, a special case of field and orientation dependence of the spontaneous polarization is analyzed.

1 Introduction

Hard magnetic materials – or permanent magnet materials: PMM – play an important role in our daily life (e.g. in our homes, cars, computers) as well as in industry. In this century many different types of PMM have been developed [1] such as the shape-anisotropy materials Fe-Cr-Co and Alnico, the extremely cheap hard ferrites and the rare-earth (R) transition-metal (T) magnets which are capable of storing a very high magnetic energy density. Certain magnetic properties of the compounds from which the PMM are produced do practically *not* depend on the microstructure of the samples. Examples for these so called intrinsic magnetic properties are the polarization measured in a large field (saturation polarization J_s), the Curie temperature T_C , quantities characterizing the magnetic anisotropy (see Sect. 2.2) *etc.* Good intrinsic magnetic properties are an important prerequisite for a compound to be a candidate for PMM. In the ideal case the intrinsic magnetic properties should be determined on single crystals of the compounds. In some cases, however, single crystals are not yet available because it is difficult to prepare them, as for example, R_3T_{29} or the interstitially modified compounds $Sm_2Fe_{17}N_3$, $Sm_2Fe_{17}C_3$, $Nd(Fe,Ti)_{12}N$ *etc.* Therefore, in this investigation fitting procedures will be used that allow to determine the intrinsic magnetic properties from demagnetization curves (DMC) of polycrystalline materials. Although $Nd_2Fe_{14}B$ single crystals are available polycrystalline samples of this compound have been included for comparison.

2 Intrinsic magnetic properties

2.1 Spontaneous magnetization

Typical magnetization-*vs.*-field curves of a PMM are hysteresis loops characterized by extrinsic magnetic properties as the coercive field H_c (or ${}_iH_c$), the remanent polarization J_r , the initial susceptibility χ_i *etc.* The nonvanishing J_r clearly indicates that a spontaneous polarization or magnetization $\vec{J}_{sp}$ is present in these materials because they are ferromagnetic as $Nd_2Fe_{14}B$ and $SmCo_5$ or ferri-

magnetic as the hard ferrites and the R-T compounds with heavy R elements. $\vec{J}_{sp}$ is an intrinsic magnetic property insofar as it is gouverned by interactions within the atoms and between them in the solid state structure. In common PMM, J_{sp} is dominated by the spin contribution of $3d$ electrons that may be localized (e.g. hard ferrites) or delocalized (e.g. $Nd_2Fe_{14}B$). The orbital magnetic moment of these electrons is usually quenched due to non-rotationally symmetric interactions within the solid. On the other hand the magnetic moment related to the total angular momentum $\mathcal{J}$ of the R ions in typical PMM is usually not quenched but stabilized by exchange interactions [2]. Among the numerous types of exchange interactions that are known to cause magnetic order in PMM based on R and/or T elements the most important ones are direct exchange between $3d$ electrons (e.g. $Nd_2Fe_{14}B$), superexchange between $3d$ electrons (through O, e.g. in hard ferrites), and indirect exchange between $4f$ electrons (via $5d$ and $3d$ electrons [3]). The extrinsic properties mentioned above are not only controlled by the atomic-scale magnetism but also by the microstructure of the considered material. This is particularly true for H_c which is extremely sensitive to details of the microstructure. Appropriate microstructures give rise to kinetic barriers that stabilize the thermodynamically metastable magnetized states against demagnetization processes as typically nucleation of reverse domains or depinning of domain walls. In this investigation we mostly assume that the magnitude of the spontaneous polarization, J_{sp}, is a function of temperature but neither depends on the direction of $\vec{J}_{sp}$ with respect to the crystallographic axes nor on the magnitude and the direction of applied field $\vec{H}_{ext}$. This is also a concept of the continuum theory called micromagnetism [4,5] where an only-temperature-dependent local polarization is introduced. The thermodynamically preferred directions of $\vec{J}_{sp}$ (in zero applied field) are called easy magnetization directions (EMD). The reason why the concept of an only-temperature-dependent J_{sp} works rather well for many ferro- as well as ferrimagnetic materials is that the isotropic exchange interactions are stronger than most of the other types of interactions influencing J_{sp}. However it is well known that, to some degree, J_{sp} depends on the applied magnetic field. Even if $\vec{H}_{ext}$ is parallel to the EMD of a simple ferromagnet J_{sp} increases with increasing H_{ext} [6]. Enhanced high-field susceptibilities and various nonlinear high-field magnetization processes appear in ferrimagnetic materials and in materials with non-collinear magnetic structures [7]. As shown theoretically [8] J_{sp} depends also on the direction of $\vec{J}_{sp}$. It should be noted, however, that it will be difficult to directly measure such a dependence because in the case of a PMM usually large fields $\vec{H}_{ext}$ are needed to turn $\vec{J}_{sp}$ from its EMD. In YCo_5 the low-temperature value of J_{sp} measured perpendicularly to the EMD is significantly smaller than that measured parallel to the EMD [9]. A similar effect was observed for $Nd_2Fe_{14}B$ at room temperature [7]. In this investigation a field dependence of J_{sp} has been found for polycrystalline $Nd_2Fe_{14}B$ and Sm_2Fe_{17} samples for temperatures not far below T_C (see Sect. 4.3).

2.2 Magnetocrystalline anisotropy

Magnetocrystalline anisotropy (MA) of a PMM refers to the dependence of its free energy on the direction of $\vec{J}_{sp}$. It is beyond the scope of this paper to describe the numerous physical mechanisms underlying the MA of the various PMM. A common aspect valid for nearly all types of PMM is that J_{sp} mainly results from the spins of the $3d$ and/or $4f$ electrons whereas the anisotropy is due to purely electrostatic effects (crystal fields) or quantum mechanical hybridization both acting on electron orbitals. Therefore spin-orbit interaction is needed to transform the orbital anisotropy to the spin moments. Exceptions are the magnetic dipol-dipol interaction being anisotropic itself and the

related internal shape anisotropy (e.g. in Alnico). Phenomenologically, the MA can be described independently of its microscopic mechanism by a power series in the direction cosines, α_i, of $\vec{J}_{sp}$

$$F = K_0 + \sum_{i,j} K_{ij}\alpha_i\alpha_j + \sum_{i,j,k,l} K_{ijkl}\alpha_i\alpha_j\alpha_k\alpha_l + \quad \ldots \tag{1}$$

where the anisotropy "constants" K_{ij}, K_{ijkl}, ... are functions of temperature but they are assumed to not depend on $\vec{H}_{ext}$ (see Sect. 2.1). For each crystal system a certain set of non-vanishing anisotropy constants exists [7]. In an alternative description being more convenient for non-cubic systems F is written as an series expansion in terms of spherical harmonics $Y_l^m \propto P_l^{|m|}\exp(im\varphi)$

$$F = \sum_{l}^{\infty} \sum_{m=-l}^{m=l} \kappa_{lm} P_l^{|m|}(\theta)\exp(im\varphi) \tag{2}$$

where κ_{lm} are the anisotropy coefficients, θ is the polar angel of $\vec{J}_{sp}$ with respect to an appropriately chosen crystallographic axis and φ the azimuth in the plane perpendicular to this axis. In R-T PMM the MA is dominated by crystal fields acting on well localized $4f$ orbitals [10]. Therefore, the ratio of the diameter of the $4f$ shell to the distance between the R site and its charge-carrying neighbors can be taken as a small parameter. Then, eq.(2) is a power series in this parameter and κ_{lm} is of (l+1)th order [11] (see Sect. 3.5). For crystallographically uniaxial materials, e.g. tetragonal, trigonal or hexagonal materials, the lowest order of F in eq.(2) does not depend on φ:

$$F = K_0 + K_1 \sin^2\theta . \tag{3}$$

Here, θ is the angle between $\vec{J}_{sp}$ and the crystallographic c-axis. For $K_1 > 0$ the c-axis is the EMD. Within the approximation (3), for materials with $K_1 < 0$ all directions perpendicular to the c-axis are EMD's. These so called easy-plane materials can not be used for PMM because they positively yield a vanishing coercive field, $H_c = 0$. For hexagonal materials also the next order omitted in eq.(3), $K_2 \sin^4\theta$, is independent of the azimuth angle and a phase diagram can be constructed distinguishing regions of (K_1, K_2) with EMD, easy-plane and easy-cone types of MA [12]. For higher order terms in eq.(2) or lower crystal symmetry the minimization of F always leads to discrete EMD's (but not easy-plane or easy-cone types of MA). From the anisotropy constants different types of anisotropy fields can be defined describing the stiffness against rotation of $\vec{J}_{sp}$ from the EMD [12]. In general, these anisotropy fields depend on the angular distance of $\vec{J}_{sp}$ from the EMD as well as the turning direction. For EMD type materials an often used definition of the anisotropy field is

$$H_A = (2K_1 + 4K_2)/J_{sp} \tag{4}$$

In that case H_A is the field which is needed to saturate a grain whose EMD is perpendicular to the applied field. There are various methods for experimental determination of the anisotropy constants on single crystals from magnetic measurements, torque measurements or ferromagnetic resonance. Very high anisotropy fields have been successfully determined by the *singular point detection* (SPD) method using pulsed magnetic fields [13]. In this study, the anisotropy constants will be determined from demagnetization curves of polycrystalline samples.

3 Basic fit procedure

3.1 Description of the fit procedure

As in earlier investigations [14, 15] the fit procedures discussed in the following sections are based on the analysis of reversible rotational processes of the local magnetization which is assumed to be homogeneous in the individual crystallites (grains) of the polycrystalline material. The orientation of the individual magnetization in a decreasing applied field (after complete saturation of the sample) can simply be described by the STONER–WOHLFARTH model [16]. To introduce the basic idea of the used fit procedure simplifying assumptions are made in this section: i) the MA of the material is uniaxial and can be sufficiently well described by two anisotropy constants K_1 and K_2, ii) the alignment of the grain's crystallographic axis to which the uniaxial MA refers (usually the c-axis) can be described by a one-parametric (parameter ξ) rotational-symmetric texture function and iii) J_{sp} depends on temperature only. These assumptions allow to investigated the majority of samples made of NdFeB or $Sm_2Fe_{17}N_3$; some generalizations to the restrictions just made will be discussed in Sect. 4. The sample polarization in dependence on field is given by the sum of the grain polarization components in field direction

$$J(H) = \frac{v J_{sp}}{2\pi} \int_{\omega=0}^{2\pi} \int_{\vartheta=0}^{\pi/2} \sin\vartheta \, f(\alpha,\xi) \cos(\vartheta - \theta) \, d\omega \, d\vartheta \tag{5}$$

where ϑ and θ denote the angles of the field direction and of $\vec{J}_{sp}$ with respect to the c-axis of the individual grain, respectively. ω denotes the azimuth angle of the c-axis (and, for the time being, of $\vec{J}_{sp}$) in a plane perpendicular to $\vec{H}$ measured to the projection of the texture axis $\vec{t}$ into that plane. The argument α of the texture function $f(\alpha,\xi)$ is the angle between the considered c-axis and the texture axis of the sample. If the angle between $\vec{H}$ and $\vec{t}$ is introduced to be τ the relation

$$\cos\alpha = \cos\vartheta \cos\tau + \sin\vartheta \sin\tau \cos\omega \tag{6}$$

holds. It should be noted, that the demagnetizing field for arbitrary sample orientation τ is not necessarily antiparallel to the applied field H_{ext}. In the cases $\tau = 0$ and $\tau = \pi/2$ (and $\vec{t}$ being one of the principal axis of the sample's demagnetization tensor), however, the demagnetization effect can approximately be taken into account by introducing the internally acting field $H = H_{ext} - D\,J$ with D being a demagnetization factor. The volume fraction v of the magnetic grains is given by the ratio of the sample saturation polarization J_S to the spontaneous polarization J_{sp} of the material. The orientation θ of J_{sp} has to be determined from the minimum of the density F of the free energy

$$F = K_1 \sin^2\theta + K_2 \sin^4\theta - J_{sp} H \cos(\vartheta - \theta) \tag{7}$$

where anisotropy constants up to fourth order for the magnetically uniaxial material are taken into account and in-plane anisotropies are neglected (cf. Sect. 2.2). It should be noted, that in general eq. (7) may have not only one minimum. In particular, for certain K_1 and K_2 so-called "first order magnetization processes" may take place [17]. These processes are taken into account in the used (inner) numerical minimization of F. Thus, $\theta(H,\vartheta)$ may depend on the magnetic history of the sample. In our analysis, only major DMC are considered, i.e. a further increase of the initially applied field H_{ext} will not result in a change of these DMC.

In order to determine the intrinsic magnetic properties of a sample the calculated polarizations $J_{\|}$ and $J_{\perp}$ are fitted to the measured demagnetization curves, $J_{\|}^{\exp}(H_k)$ and $J_{\perp}^{\exp}(H_k)$, for fields $\bar{H}$ applied parallel and perpendicular to the sample texture axis, respectively. This outer minimization has to be normalized by the accuracies $\Delta J_{\|}^{\exp}(H_k)$ and $\Delta J_{\perp}^{\exp}(H_k)$ of the k-th measurement performed at $H = H_k$

$$\sum_{k=1}^{n} \sum_{\varepsilon=\|,\perp} \frac{\left(\left[J_{\varepsilon}(K_1, K_2, J_s, \xi, H_k) + \chi_p H_k + J_w\right] - J_{\varepsilon}^{\exp}(H_k)\right)^2}{\Delta J_{\varepsilon}^{\exp}(H_k)} = \chi_m^2 \rightarrow Min. \qquad (8)$$

Here, $\chi_p H_k$ and J_w are polarization contributions by paramagnetic or soft phases, respectively, which can not be excluded to be present inside the sample additionally to the magnetic main phase. A further cause for a non-zero χ_p will be discussed in Sect. 4.3. Eq.(8) leads to a 6-dimensional minimization problem of χ_m^2. However, introducing $k_1 = K_1 / J_s$ and $k_2 = K_2 / J_s$, the parameters J_S, χ_p and J_w can be calculated by a routine for linear problems which saves efficiently computation time. Only the three parameters k_1, k_2 and ξ have to be calculated by a non-linear minimization procedure. In the used procedure, each parameter can be fixed to a given value (e.g. if the amount of soft magnetic α-Fe in a sample is known by X-ray measurements) or to a certain interval. In order to minimize influences of demagnetization effects on the measured polarization values and, in particular, to exclude nonhomogeneous states of magnetization (domains) only those values of the polarization measurements with decreasing applied field were fitted for which $\mu_0 H \geq 1.5$ T. Note that from the point of view of statistics the residual sum χ_m^2 of the deviations between measured and calculated polarization values defined by eq.(8) is claimed to be less than unity [18]. Only in this case the applied model of reversible polarization rotation can be considered as valid.

3.2 Texture of magnetic samples

As discussed in Sect. 2, the intrinsic magnetic properties of a material do (nearly) not depend on its microstructure. However, the rotational magnetization processes utilized in this study for the determination of the intrinsic properties depend on the orientation of the individual grains in the sample and hence, on the texture of the considered material (cf. eq.(5)). Therefore, in our fit procedure information on texture has to be treated simultaneously with purely magnetic data. For a magnetically uniaxial material only the alignment of the c-axes is of interest. If during the preparation of the polycrystalline material only one direction is preferred and if the preparation process can be considered as a statistical one with neglegable interaction of the grains a Gaussian distributed density of the c-axes is expected,

$$f(\alpha, \sigma_g) \propto \exp\left(-\frac{(\alpha - \alpha_0)^2}{2\sigma_g^2}\right) \qquad 0 \leq \sigma_g < \infty \qquad (9)$$

Here, α_0 is the angle at which f has its maximum and $\sigma_g = \xi$ is the texture parameter of eq.(5). If a sample is prepared by powder compaction in an aligning field, α_0 corresponds to the zero-field magnetization orientation θ at the preparation temperature. Depending on the anisotropy constants α_0 is, in particular, given by:

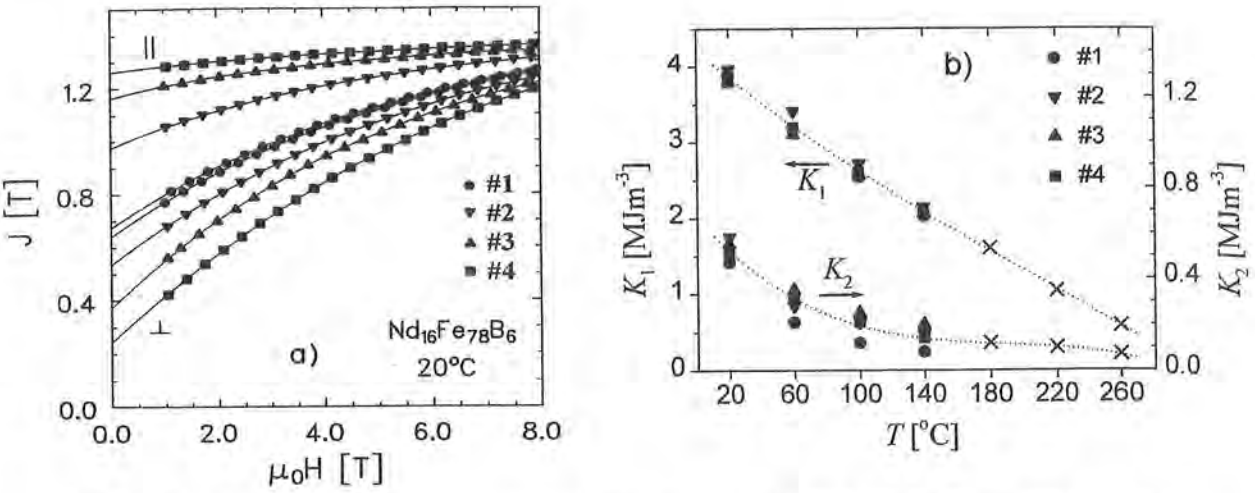

Fig.1: a) Measured (markers) demagnetization curves of four NdFeB samples (#1...#4) at room temperature with their texture axes parallel and perpendicular to the measuring field. The lines have been calculated from the fit results. b) Anisotropy constants as derived by fitting to DMC measured at different temperatures. The high temperature data (×) are included for comparison; their determination is discussed in Sect. 4.3.

$\alpha_0 = 0$	for	$K_1 > 0$ and $K_2 > -K_1$	(EMD)
$\alpha_0 = \arcsin\sqrt{-K_1/2K_2}$	for	$K_1 < 0$ and $K_2 > -K_1/2$	(easy cone)
$\alpha_0 = \pi/2$	for	$K_2 < -K_1/2$	(easy plane)

Note that application of a rotating field during the powder compaction of an easy plane material results in $\alpha_0 = 0$. Texture functions according to eq.(9) were used in investigating samples by means of different methods [14, 19, 20]. A confirmation of the applicability of eq.(9) will be presented in Sect. 4.2. Alternative descriptions of texture can be given by a FOURIER series expansion [21, 22]. For comparison of different texture functions $f(\alpha,\xi)$ a common parameter must be found which is in well defined correlation with ξ. Empirical texture parameters (e.g. the remanence ratio) are not much useful since they depend not only on texture but also on grain interactions. A more suitable quantity is the standard deviation σ of the angle α

$$\sigma^2 \equiv \overline{(\alpha^2 - \bar{\alpha}^2)} = \int_0^{\pi/2} \sin\alpha\, f(\alpha,\xi)\,(\alpha-\bar{\alpha})^2\, d\alpha \ . \tag{10}$$

In Sect. 4.2 also non-rotationally symmetric texture functions will be taken into account.

3.3 Application of the basic fit procedure to material of easy axis anisotropy

In the following, four $Nd_{16}Fe_{78}B_6$ samples are investigated prepared from the same parent alloy and heat treated under the same conditions but aligned in static fields of different strengths. From this, the same intrinsic magnetic properties of these samples but different degrees of grain alignment are expected [23]. The results of the fitting procedure are shown in Fig. 1.a where the calculated polarization values (lines) are compared to the values measured (markers) at room temperature for $\tau = 0$ ($\parallel$) and $\tau = \pi/2$ ($\perp$) . Only each third polarization value is presented for clarity. For the shown fit-

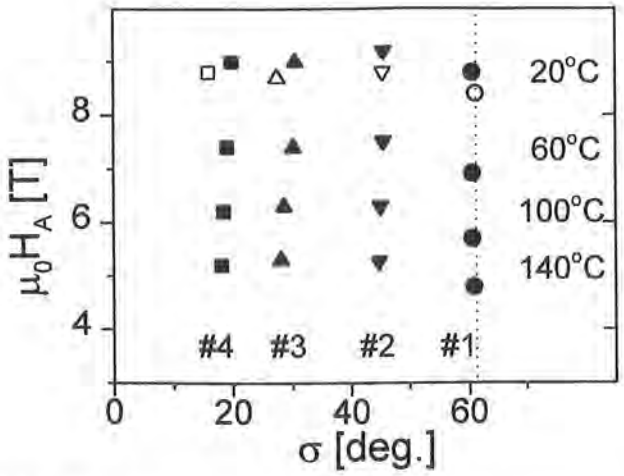

Fig.2: Anisotropy fields H_A of four samples of Fig. 1 at four temperatures in dependence on the texture parameter σ defined in eq.(10). In such a presentation the markers should form a grid since the results for H_A are expected to depend on temperature only whereas σ may vary for different samples but not with temperature. Open symbols display results of comparative SPD measurements. (Dashed line: limit of isotropic samples.)

ting results we have $\chi^2_m \approx 0.7$. The anisotropy constants K_1 and K_2 as derived from these fits are presented in Fig. 1.b. The consistence of the results obtained by the fit as well as an overview is given in Fig. 2 where the anisotropy fields (as defined in eq.(4)) at four temperatures and the texture parameters σ of the four samples are presented. The texture parameter obtained for an individual sample should not depend on temperature and hence, the corresponding results for each sample should lie on lines parallel to the H_A-axis. Furthermore, the anisotropy field is expected to depend on temperature only and should not be influenced by the degree of grain alignment. Therefore, the H_A-values of these four samples at fixed temperature are expected to form parallels to the σ axis. Both demands are clearly complied with the results shown in Fig. 2 supporting the applicability of the used fitting procedure. Note that the fit results for H_A and σ at room temperature agree with the values obtained by SPD for the same set of samples [23].

Demagnetization curves of $Sm_2Fe_{17}N_3$ have been analyzed using the same idea of investigation of differently textured samples at different temperatures. For this aim, $Sm_2Fe_{17}N_3$ samples were prepared from the same powder but, again, fields of different strength were applied while compacting the powder [15]. The resulting demagnetization curves obtained for three samples at room temperature are shown in Fig. 3 and compared with the fitted $J(H)$-curves. The maximum deviation between measured and calculated polarization values is less than 2 mT. The results of these fits are discussed in Sect. 3.5. The influence of the stray field on the measured polarization values is clearly visible in the low field region ($\mu_0 H < 1$ T) in Fig. 3. Since only the averaged demagnetizing field is taken into account in the fitting procedure the polarization values measured at fields $\mu_0 H < 2$ T were not used.

3.4 Material of non-easy axis anisotropy

In the following, a polycrystalline Sm_2Fe_{17} sample prepared by grain alignment in a static field is investigated. The material is known to have easy plane MA. In order to examine the applicability of the fit procedure to material without easy axis MA, α_0 was not just set to be $\pi/2$ but was treated as

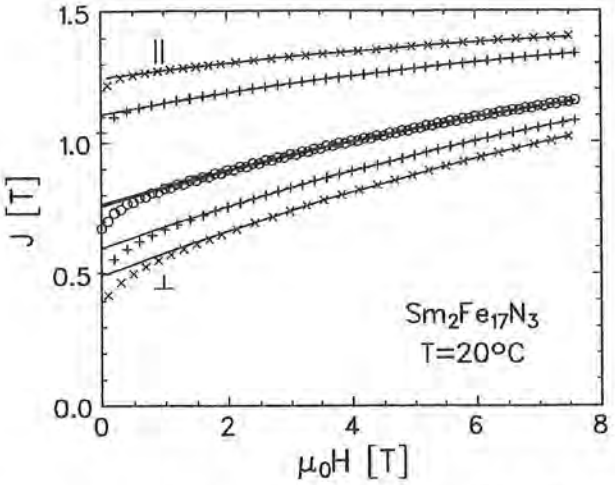

Fig.3: Demagnetization curves of three different textured $Sm_2Fe_{17}N_3$ samples measured (markers) and fitted (lines) for texture axis parallel ($\parallel$) and perpendicular ($\perp$) to the measuring field. The deviations at low field show the influence of the stray field.

an open fit parameter. In this case, the parameter J_w was omitted for keeping the number of open parameters (unnitrided Sm_2Fe_{17} can be produced without containing α–Fe for which J_w was mainly included). The maximum deviation of 2 mT between measured and fitted demagnetization curves at room temperature (not shown here) indicated a successful fit. The fitted parameters are: $K_1 = -2.05$ MJm^{-3}, $K_2 = 0.42$ MJm^{-3}, $\sigma_g = 35.2°$, $J_S = 1.12$ T, $\chi_p = 5.5 \cdot 10^{-9}$ $VsA^{-1}m^{-1}$, $\alpha_0 = 89.9°$. The value of α_0 quite close to $\pi/2$ corresponds to the values of K_1 and K_2 (easy plane MA) confirming the consistence of the fitting procedure. The value of K_1 differs little from that given in [14]. Applying a rotating magnetic field during resin bonding [24] allows to produce textured samples with $\alpha_0 = 0$ from material of easy plane MA, i.e., also for such material a maximum number of grains can be aligned with their *c*-axes parallel to the texture axis. By means of this method, however, the powder can not be compacted during the grain alignment and hence, samples of high density can not be produced. By application of a rotating field textured Sm_2Fe_{17} and $Dy_2Fe_{17}N_3$ samples have been prepared. For the former sample [24], the fit yields $K_1 = -2.1$ MJm^{-3}, $K_2 = 0.4$ MJm^{-3} and $J_{sp} = 1.12$ T in excellent agreement with the results above. The results [25] for the Dy-containing sample are $K_1 = -3.0$ MJm^{-3}, $K_2 = 0.0$ MJm^{-3} and $J_{sp} = 1.12$ T, the latter being in agreement with the value given in [26]. The texture parameter has been determined to $\sigma_g = 28°$ using a Gaussian texture function.

3.5. Interpreting results for $Sm_2Fe_{17}Z_x$ (Z = N, C, H): the Crystalline Electric Field

In this section the results obtained for the anisotropy constants of the interstitially modified 2:17 compounds [27] will be exploited to analyze the parameters of the crystalline electric field (CEF). The strong increase of the MA of the $R_2Fe_{17}Z_x$ compounds compared to the non-modified case (x = 0) is originated by the CEF of the interstitial atoms Z (N, C, or/and H) acting on the aspherical 4*f* electron shell of the rare earth R. This anisotropy is transferred via 4*f*–5*d* exchange coupling and hybridization to the 3*d* electrons of the iron and hence to the spontaneous polarization. Starting from this picture the Hamiltonian of a single R-ion [25, 28, 29] is given by

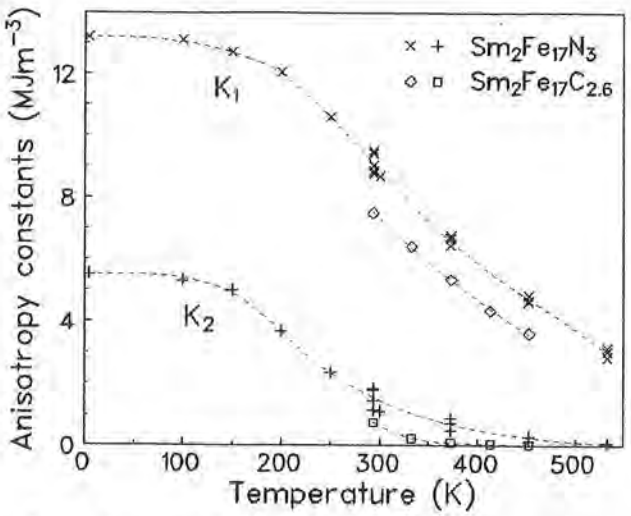

Fig.4: Temperature dependences of the anisotropy constants K_1 and K_2 determined experimentally from several $Sm_2Fe_{17}N_3$ and $Sm_2Fe_{17}C_{2.6}$ samples.

$$\mathcal{H} = 2(g-1)\mu_B \mathcal{J} n_{RFe} \vec{J}_{sp}(T) + \sum \theta_n A_{nm} \langle r^n \rangle \hat{O}_n^m \tag{11}$$

where the applied field is taken into account via the orientation of $\vec{J}_{sp}(T)$. The exchange field is expressed within a mean field approximation by the molecular field coefficient n_{RFe} and the net magnetization $\vec{J}_{sp}(T)$ due to the moment of the Fe sites ($\mathcal{J}$ is the total angular momentum of R and g its LANDÉ factor; μ_B - BOHR magneton). The STEVENS operators $\hat{O}_n^m$, the STEVENS coefficients θ_n and the averaged n-th power of the 4*f* radius, $\langle r^n \rangle$, refer to the R-ion, whereas the CEF (expressed by A_{nm}) is mainly due to the interstitial atoms. According to the structure of 2:17 compounds, A_{20}, A_{40} and A_{60} have to be taken into account if in-plane anisotropies are neglected. Comparing the angular dependences as given in eqs.(2) and (11) within a linear approximation [30] results in

$$\begin{aligned} K_1 &= -\tfrac{3}{2}\kappa_{20} - 5\kappa_{40} - \tfrac{21}{2}\kappa_{60} + K_1^{Fe} \\ K_2 &= \tfrac{35}{8}\kappa_{40} + \tfrac{189}{8}\kappa_{60} \\ K_3 &= -\tfrac{231}{16}\kappa_{60} \end{aligned} \tag{12}$$

where the κ_{lm} are given by

$$\kappa_{n0} = N_R \theta_n A_{n0} \langle r^n \rangle \langle O_n^0 \rangle_T \,. \tag{13}$$

N_R is the density of the R ions and K_1^{Fe} is the 3*d* anisotropy contribution as determined from $Y_2Fe_{17}N_3$. The thermal averages of the operator equivalent $\langle O_2^0 \rangle_T$ can be calculated i) for zero temperature [11] where $\mathcal{J}$ can be substituted by $\mathcal{J}_z$ or ii) for arbitrary temperature [25] via the generalized BRILLOUIN functions [30] with $2|g-1|\mu_B \mathcal{J} n_{RFe} J_{sp}(T)/k_B T$ as argument. The results for K_1 and K_2 as provided by the fit procedure are perfectly suitable for the determination of A_{20} and A_{40}. Note that this calculation yields more reliable results for the CEF parameters than the mere use of aniso-

compound	J_{sp} [T]	A_{20} [Ka_0^{-2}]	A_{40} [Ka_0^{-4}]
Sm_2Fe_{17}	1.12	35	0
$Sm_2Fe_{17}H_4$	1.34	110	42
$Sm_2Fe_{17}C_{2.6}$	1.45	-310	66
$Sm_2Fe_{17}N_3$	1.54	-410	72
$Dy_2Fe_{17}N_3$	1.12	-170	/

Table 1: Spontaneous polarization J_{sp} (at $T = 293$ K) and CEF parameters A_{20} and A_{40} for different 2:17 compounds (a_0 - Bohr's radius).

tropy field data [28, 31]. Data for K_1 and K_2 of $Sm_2Fe_{17}N_3$ and $Sm_2Fe_{17}C_{2.6}$ as determined by the fit procedure and used in the following are shown in Fig. 4. In the case of R = Sm, the ground state is given by $\mathcal{J} = 5/2$ and hence, A_{60} and correspondingly K_3 vanish. Although higher values of $\mathcal{J}$ [28, 29] ought to be taken into account their neglect is expected to cause minor inaccuracies only since $\mathcal{J}$-mixing and non-linear effects have opposite influence [30] on A_{20}. The CEF parameters were calculated from eq.(12) and are summarized in Tab. 1. The increase of J_{sp} for the interstitially modified Sm-compounds is not only caused by the changed magnetic moment of the iron atoms but mainly by the increased exchange coupling giving rise to an enhanced T_C. Starting from the parent compound, the leading parameter A_{20} is changed in opposite directions by interstitial modification with H or N/C, respectively, due to [32] opposite trends in the change of the rare earth valence electron density in the plane containing R and interstitial atoms for H and N/C. Considering only relative electronegativity (as, e.g., in the screened charge model) our result shows the "electropositive" character of hydrogen whereas N and C are strongly electronegative. For $Dy_2Fe_{17}N_3$ ($\mathcal{J} = 15/2$) only a crude estimation is obtained since K_3 had to be determined (cf. Sect. 5) and the argument of the BRILLOUIN function is shifted to lower, more inaccurate values. However, no $\mathcal{J}$-mixing is expected for Dy. The fact that A_{20} does not much vary for $Sm_2Fe_{17}N_3$, $Sm_2Fe_{17}C_{2.6}$ and $Dy_2Fe_{17}N_3$ in Tab. 1 can be considered as a fair result [25].

4 Adaptation and generalization of the basic fit procedure

4.1 Anisotropy of monoclinic ferromagnetic compounds

Compounds of composition R_3T_{29} or the interstitially modified phases $R_3Fe_{29}N_x$ reveal a monoclinic crystalline structure which can be derived from the 1:5 parent $CaCu_5$-type structure by replacing 2/5 of the R atoms by Fe dumb-bells [33]. This represents an intermediate structure between the rhombohedral 2:17 and the tetragonal 1:12 structure and can formally be written as

$$R_3T_{29} = R_1T_{12} + R_2T_{17}\,. \tag{14}$$

In the 3:29 compounds as well as their corresponding interstitial modifications, the R ions in one type of segment have nearly the same environment as in the rhombohedral R_2Fe_{17} structure, whereas their environment in the other type of segment is the same as in the tetragonal RT_{12} [33, 34]. These structural relationships are maintained upon nitrogenation while the Curie temperature increases. Considering the local environment of, e.g., Sm in $Sm_3(Fe,Ti)_{29}N_4$ with regard to the interstitial N atoms, 2 Sm atoms with a 1:12 environment and 4 Sm atoms with a 2:17 surrounding per unit cell are found. For the following description of MA in the 3:29 structure it is convenient to introduce two axes c_r and c_t defined as the c-axes of the rhombohedral (r) 2:17 and tetragonal (t) 1:12 seg-

ments, respectively. These axes, together with the two-fold b_m axis of the monoclinic (m) structure, form a Cartesian coordinate system. For the two types of segments the *lowest* (i.e. second) order term of the anisotropy energy density F_A in eq. (3) is now given by $K_{1,t} \sin^2\theta_t$ and $K_{1,r} \sin^2\theta_r$, respectively. Here, θ_t and θ_r are the polar angles of the local spontaneous polarization with respect to the axes c_t and c_r, respectively, and $K_{1,t}$ and $K_{1,r}$ are the corresponding anisotropy constants. For a calculation of F in the 3:29 structure a superposition of the anisotropy contributions of the two segments is assumed and and a unified set of angular variables has to be introduced. In our description of the monoclinic system the polar angle θ is measured with respect to the (former) c_r-axis and the azimuth angle φ to the (former) c_t-axis. This results in

$$F = \frac{2v_r}{3v_m} K_{1,r} \sin^2\theta - \frac{v_t}{2v_m} K_{1,t} \sin^2\theta\,(1+\cos 2\varphi)\,. \tag{15}$$

The factors $2v_r/3v_m$ and $v_t/2v_m$ (v_r/v_m, v_t/v_m – volume ratios of the different segments) weight the energy contributions of the R^{3+} ions in the two different segments with respect to their corresponding volume. The angular dependences in eq.(15) reflect that the MA of the 1:12 and the 2:17 segment refer to different crystallographic axes in the 3:29 structure. For nitrided $Sm(Fe,Ti)_{12}N$ and $Sm_2Fe_{17}N_3$ it is well known that $K_{1,t} < 0$ and $K_{1,r} > 0$, respectively. Hence, for $Sm_3Fe_{29}N_4$ the axes c_t and c_r are the hard and easy magnetization directions, respectively [35]. For a more general description of a monoclinic system we have

$$F = K_{1\theta} \sin^2\theta + K_{1\varphi} \sin^2\theta(1+\cos 2\varphi) \tag{16}$$

where the angle θ of J_{sp} corresponds to one of the three principal axes of an energy ellipsoid (including the monoclinic b_m-axis). In the general case, each of these axes can be EMD. Our fit procedure automatically relates θ (and consequently $K_{1\theta}$) to the EMD, independently of the EMD's crystallographic orientation, whereas $\theta = \pi/2$, $\varphi = 0$ corresponds to the magnetically hard direction. Which of the crystallographic directions is related to the easy and hard magnetization direction depends on the specific type of crystallographic structure and the rare earth under investigation. Thus, magnetization measurements which refer to eq.(16) need to be accompanied by additional information (as shown above for $Sm_3(Fe,Ti)_{29}N_4$) to assign the magnetic axes to crystallographic ones. This assignment is required for the calculation of anisotropy constant related to crystallographic axes (as c_t and c_r above) from the formally introduced $K_{1\theta}$ and $K_{1\varphi}$. For an investigation of the reversible rotational processes in materials of monoclinic structure eq.(7) has to be replaced by

$$F = K_{1\theta} \sin^2\theta + K_{1\varphi} \sin^2\theta(1+\cos 2\varphi) - H J_{sp} \cos\eta \;\Rightarrow\; Min. \tag{17}$$

Here, η denotes the angle between the field (applied at a polar angle ϑ with respect to the EMD and an azimuth Φ with respect to the b_m-axis) and J_{sp}. Eq.(17) features a completely different rotational behavior of the polarization if compared with eq.(7) due to the fact that $K_{1\theta}$ and $K_{1\varphi}$ can be of the same order of magnitude. The behavior of grain polarization is illustrated in Fig. 5 where the values

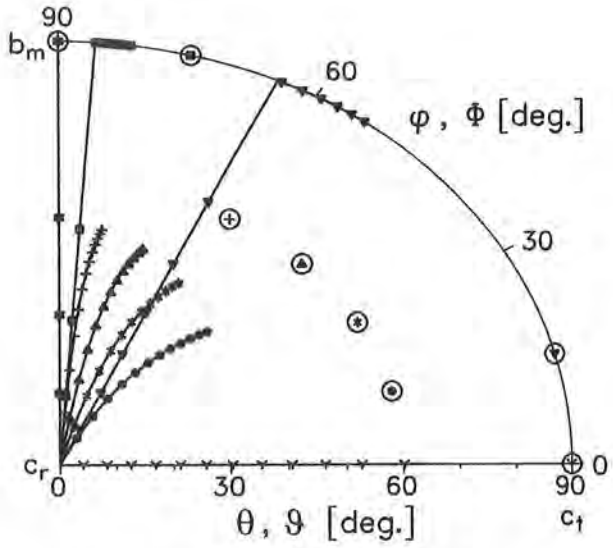

Fig.5: Polar presentation of the calculated rotation of the polarization of a $Sm_3(Fe,Ti)_{29}N_4$ single crystal in an increasing fields. c_r and c_t are the magnetically easy and hard direction, respectively. The polar angles of magnetization (θ) and field (ϑ) are related to the EMD pointing out of the page. The corresponding azimuth angles, φ and Φ, vary from 0° (c_t-axis) to 90° (b_m-axis). The solutions for every 2 T of field magnitude are presented by markers. Field directions are indicated by corresponding circled markers. Note that the polarization direction may strongly deviate from an in-plane rotation.

$K_{1\theta} = 4$ MJm^{-3}, $K_{1\varphi} = 5.2$ MJm^{-3} and $J_{sp} = 1.3$ T were used. These values as well as the chosen axes assignment (c_r as the EMD) resemble $Sm_3(Fe,Ti)_{29}N_4$. From this polar presentation of the polarization orientation it is obvious that three cases of the applied field direction can be distinguished: i) polar angle $\vartheta = 90°$ and azimuth angle $\Phi = 0°$ or 90°: the grain polarization rotates like in a uniaxial material with anisotropy fields $\mu_0 H_{A1} = (2K_{1\theta} + 4K_{1\varphi}) / J_{sp}$ (for $\Phi = 0°$) and $\mu_0 H_{A2} = 2K_{1\theta} / J_{sp}$ (for $\Phi = 90°$). ii) $\vartheta = 90°$ and $0° < \Phi < 90°$ ($\Phi = 15°$ and 75° shown): the polarization rotates with fixed $\varphi > \Phi$ toward the plane perpendicular to the EMD for field smaller than a specific field $H_{A\varphi}$ where $H_{A1} < H_{A\varphi} < H_{A2}$. For increasing fields higher than $H_{A\varphi}$ the polarization rotates in the plane perpendicular to the EMD toward the field direction but is never parallel to the field for finite field strength. iii) For arbitrary field direction $0° < \vartheta < 90°$ ($\vartheta = 60°$, $\Phi = 15°$, 30°, 45° and 60° shown): the polarization rotates out of the EMD on curves which can be considerably bent. This bending increases the spherical angle between J_{sp} and the axis of strongest anisotropy, i.e. φ can be much larger than Φ. Since our 3:29 samples were prepared in an aligning field the distribution of the EMD with respect to texture axis is assumed to be given by eq.(9) again. A preferred alignment of the grains' hard magnetization direction (which is now also of interest) is unlikely and therefore, their orientation is assumed to be random. With this, fits of DMC's measured for fields from 7.5 T - 1.6 T were conducted. A maximum deviation between measured and calculated polarization values of less than 3 mT and a typical residual standard deviation of 0.55 $(\text{mT})^2$ accounts for the applicability of the used description. The results are presented in Tab. 2. The values for J_{sp} are in agreement with those given elsewhere [33]; the one for $Pr_3(Fe,Ti)_{29}N_4$ was taken from [33] because of an unknown dilution of the magnetic phase in this sample.

As already pointed out, for an assignment of the magnetic to the crystallographic axes additional information is needed. In case of the nitrided compounds the MA is dominated by the N atoms (cf. Sect. 3.5) and the direction of the EMD can be derived from the superposition principle discussed

sample	$K_{1\theta}$ [MJm^{-3}]	$K_{1\varphi}$ [MJm^{-3}]	$K_{1,r}$ [MJm^{-3}]	$K_{1,t}$ [MJm^{-3}]	J_{sp} [T]	σ_g [deg.]
$Sm_3(Fe,Ti)_{29}$	1.4	0.4	/	/	1.13	35
$Nd_3(Fe,Ti)_{29}$	0.3	0.3	/	/	1.32	48
$Pr_3(Fe,Ti)_{29}$	0.5	1.3	/	/	1.21	102
$Ce_3(Fe,Ti)_{29}$	0.6	2.3	/	/	0.95	116
$Sm_3(Fe,Ti)_{29}N_4$	2.9	2.4	4.4	–12.0	1.30	39
$Nd_3(Fe,Ti)_{29}N_4$	2.2	2.3	–6.9	5.5	1.54	49
$Pr_3(Fe,Ti)_{29}N_4$	1.7	3.2	–9.6	4.3	1.56*	57

Table 2: Results for the room temperature values of $K_{1\theta}$, $K_{1\varphi}$ and J_{sp} and for the texture parameter σ_g of samples prepared from $R_3(Fe,Ti)_{29}$ and their nitrides as obtained by fitting of demagnetization curves of these monoclinic materials. An assignment of magnetic to the crystallographic axes can reasonably be done so far only for the nitrides and results in the intrinsic anisotropy constants $K_{1,r}$ and $K_{1,t}$. (* from [33]).

above and the sign of the STEVENS coefficient of the rare earth. The example of R = Sm was discussed above and the comparison of eqs.(15) and (16) yields $K_{1\theta} = (2v_r/3v_m)K_{1,r}$ and $K_{1\varphi} = -(v_t/2v_m)K_{1,t}$. In comparison, for R = Nd, Pr the magnetic axes are exchanged with respect to the crystallographic ones with c_t and c_r being the easy and the hard magnetization direction, respectively. This results in $K_{1\theta} = (v_t/v_m)K_{1,t}$ and $K_{1\varphi} = -(v_r/3v_m)K_{1r}$. From Tab. 2 it is evident that introduction of N into the 3:29 structure changes the magnetic properties similarly as in the 2:17 and 1:12 structure (cf. Sect. 3.5). As an indication for the applicability of the introduced model, the values of $K_{1,r}$ for the compounds $Sm_3(Fe,Ti)_{29}N_4$ and $Nd_3(Fe,Ti)_{29}N_4$ agree in sign and order of magnitude with the K_1 determined for the $Sm_2Fe_{17}N_3$ and $Nd_2Fe_{17}N_{2.7}$, respectively.

4.2 Biaxial texture

In this section we generalize the texture description to a non-rotationally symmetric case. To limit the number of parameters uniaxial (*c*-axis) MA is assumed. Then, the simplest case of a biaxial texture function contains two free parameters describing the polar and azimuth dependence of the orientation distribution of the grains *c*-axes, respectively. Here, the presence of a polar axis – a main texture axis – is presumed. The polar dependence of the texture function is, again, assumed to be a Gaussian distribution (9)

$$f(\alpha,\psi) \propto \exp\left(-\frac{\alpha^2}{2\sigma(\psi)^2}\right) + p_i \tag{18}$$

where standard deviation σ now depends on the azimuth angle ψ. This angular dependence is assumed to be elliptical [36], i.e.

$$\frac{1}{\sigma(\psi)^2} = \frac{\cos^2\psi}{\sigma_x^2} + \frac{\sin^2\psi}{\sigma_y^2} \tag{19}$$

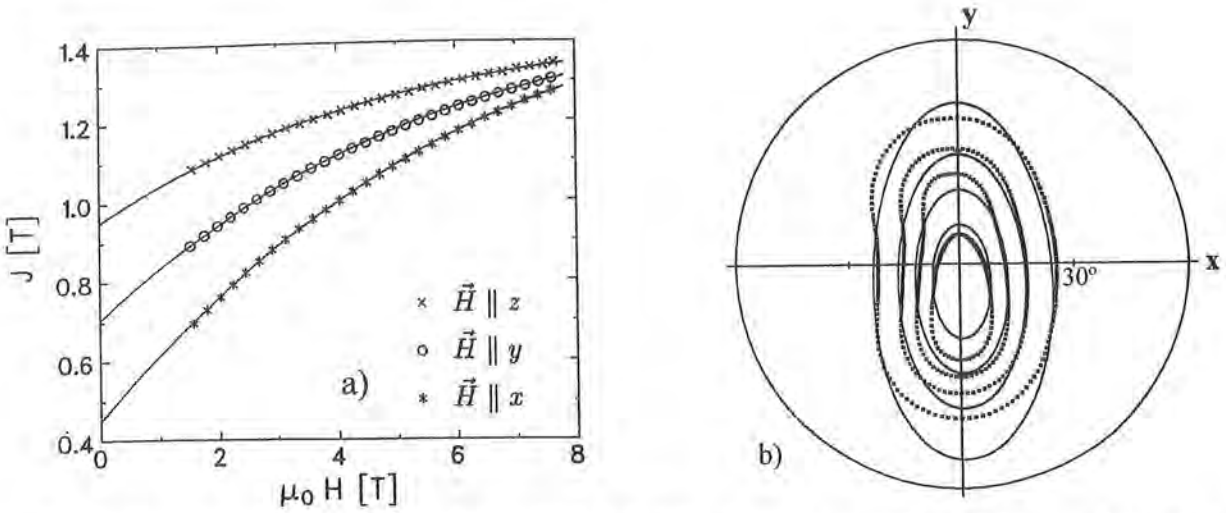

Fig. 6: Results obtained from a hot rolled $Nd_{15}Dy_{1.5}Fe_{77.5}B_6$ sample. a) Measured (markers) and fitted (lines) DMC for three orthogonal sample orientations. b) Pole figures determined from X-ray data, showing the sample's texture distribution. The markers represent values of constant *c*-axis orientation distribution. For comparison with magnetic measurements these data were fitted to a biaxial Gaussian distribution (lines).

with the parameters (main axes) σ_x and σ_y. Additionally, a possible portion p_i of isotropically distributed grains is taken into account. In the following we investigate NdDyFeB samples prepared by the hot rolling technique [37]. Caused by the columnar microstructure of the NdDyFeB alloy most of the grains were aligned with their *c*-axis parallel to the pressure direction while rolling. Hence, the texture (z-) axis of the sample is formed perpendicularly to the rolling plane. The x- and y-axis lie in the rolling plane and have been chosen perpendicular and parallel to the rolling direction, respectively. DMC were measured for three sample orientations. Comparing the two directions perpendicular to the main texture axis (Fig. 6.a) the polarization values measured in y-direction are clearly higher than those for the x-direction indicating a more pronounced grain alignment along the rolling direction. Eqs.(18) and (19) have now been used in the fit procedure instead of eq.(9). Note that the increased number of fit parameters (three texture parameters) is accompanied by more input information due to the third essential sample orientation in which independent polarization measurements can be performed. Fig. 6.a shows a good agreement between measured (markers) and fitted (lines) polarization values with a maximum deviation of 2.5 mT. The fit procedure results in J_{sp} = 1.43 T and $\mu_0 H_A$ = 8.5 T in agreement with values measured for single crystals [38] and given in Sect. 3.3. The magnetically determined texture parameters are $\sigma_x = 19°$, $\sigma_y = 53°$ and $p_i = 0.29$, the latter resulting in a sample volume of 18% being non-textured. For comparison, the pole figure for the magnetically easy axis (*c*-axis) was determined from X-ray measurements (Fig. 6.b, markers). Pole figures of reflections along (001) can not directly be measured. Each "chain" of markers corresponds to a constant value of the orientation distribution of the basal plane (001) with respect to the sample orientation. The values presented in Fig. 6.b are 5/6 (innermost "chain" of markers), 2/3, 1/2 and 1/3 of the maximum value of the orientation distribution, respectively. In order to enable a direct comparison of the texture determined magnetically to the results of X-ray measurements the (001) X-ray peak intensities (Fig. 6.b) were fitted using again the biaxial texture function defined by eqs.(18) and (19). Therein, not only the four "chains" of markers shown in Fig. 6.b but the orientation densities for the complete hemisphere were taken into consideration. The results show clearly (Fig. 6.b, lines) that the described elliptical texture is applicable for samples prepared by hot rolling.

aligning field	magnetic measurements		X-ray analysis	
$\mu_0 H_t$ [T]	σ_x [deg.]	σ_y [deg.]	σ_x^* [deg.]	σ_y^* [deg.]
0.0	127.3	183.1	120.4	166.3
0.05	28.5	43.8	29.4	40.9
2.0	10.6	15.2	11.9	15.5

Table 3: Texture parameters of the three $Nd_{14.9}Fe_{77.7}Al_{1.5}B_{5.9}$ samples determined by fitting of demagnetization curves and X-ray measurements.

Furthermore, the maximum of the texture function is only slightly shifted (about 6°) shifted toward the rolling direction y whereas the larger major axes of the ellipse described by eq.(19) are aligned exactly parallel to y (less than 2° misorientation). This pole figure analysis provides a second set of texture parameters: $\sigma_x^* = 18°$ and $\sigma_y^* = 36°$. The noticeable difference of the values σ_y^* and σ_y can be explained by the steep decrease of the orientation distribution in the range of $25° \leq \alpha \leq 40°$ (cf. markers in Fig. 6.b) which can not be modeled by a Gaussian. However, it is not surprising that the grain alignment during hot rolling, in rolling direction, can not be described statistically as assumed for a Gaussian eq.(18). Having set up the description of biaxial texture it is tempting to check on the rotational symmetry of the texture in field aligned samples. Moreover, a comparison of the magnetic and X-ray texture determination has been performed. For this aim, several differently textured $Nd_{14.9}Fe_{77.7}Al_{1.5}B_{5.9}$ samples were pressed from the same powder in magnetic fields $\mu_0 H_t$ ranging from 0 T to 2.0 T. Note that the aligning field was applied perpendicular to the press direction. As shown by X-ray analysis the main texture axes of the sample fit with the geometry given by the pressure and H_t directions. Additionally, this analysis confirmed the Gaussian eq.(9) as a feasible texture description of field aligned samples with the main texture axis defined by H_t. Fits of DMC measured along the three main texture axes of these samples yield anisotropy fields of $\mu_0 H_A = 8.4$ T. The results for the texture parameters of three samples are compared to those of X-ray analyses in Tab. 3. The good agreement confirms the texture parameter determination by the introduced fit of DMC. Note the texture formation in a field as small as $H_t = 0.05$ T. As not shown here, the degree of grain alignment remarkably increases with increasing aligning field up to $H_t \approx 0.5$ T and improves only slightly for $H_t > 1$ T. The samples show a slight non-rotational symmetry in their grain alignment. The powder compaction by uniaxial pressing may influence the texture. A higher alignment of *c*-axes is found in the press direction than in the direction perpendicular to both H_t and the press direction. However, compared to the grain alignment by the field H_t the alignment due to the pressure can be considered as small. In case of $H_t = 0$ T, i.e. powder compaction without applied field, the values of σ_x and σ_y in Tab. 3 represent a weak texture in press direction.

4.3 Field and orientation dependence of the spontaneous polarization

A detailed study of DMC of polycrystalline NdFeB samples measured well above room temperature revealed deviations between measured and fitted polarization values which become more significant with increasing temperature. As an example, the best fit of DMC measured at 533 K shows deviations of more than 10 mT making the fit unacceptable. These findings are accompanied by two observations at higher fields: i) a persistent high field susceptibility $\chi_{hf} = \mu_0^{-1} \mathrm{d}J / \mathrm{d}H$ which can not be explained by simple rotational processes and ii) a remaining difference $\Delta J_{sp}^{\parallel\perp}$ between the polarization values measured for sample texture axis parallel and perpendicularly to the field. For illustration, high field magnetization curves of a sintered well textured $Nd_{16}Fe_{78}B_6$ sample measured

at 330 K ($\mu_0 H_A \approx 7.2$ T at 330 K) and high temperature DMC (533 K) are presented in Fig. 7 (markers). These findings seem to be consistent with the behavior of $Nd_2Fe_{14}B$ single crystals [7] as discussed in Sect. 2.1. A qualitatively similar behavior was found for Sm_2Fe_{17} but not for $Sm_2Fe_{17}N_3$ (for $T \leq 533$ K). Small field dependences of J_{sp} may originate from an induced iron-sublattice moment and a changing density of states at the Fermi level (STONER model). In addition, the orbital momentum of the 4*f* electrons may slightly differ in different directions. In the following, the experimentally found values of χ_{hf} and $\Delta J_{sp}^{\parallel\perp}$ as well as their temperature dependences are analyzed within a thermodynamic model based on the idea [8] that the MA acts stabilizing against thermal fluctuations for magnetic moments oriented along the EMD. This effect should be observable for temperatures T not too far below T_C. A system of identical, well localized magnetic atoms/ions is assumed (the temperature dependence of J_{sp} for non-localized magnetic moments can also be well described if $\mathcal{J}$ is appropriately chosen). The energy density u of the magnetic system is given by

$$u = -\tfrac{1}{2}\mu_B \rho n m_J^2 J_{sp}^0 - \mu_0 \mu_B \rho m_J H \cos(\vartheta - \theta) + (\sin^2\theta - \tfrac{2}{3}) K_1(m_J, T) \tag{20}$$

where ρ is the density of magnetic moments and m_J the ratio of the spontaneous polarization to its value J_{sp}^0 at zero temperature and zero field. In mean (molecular) field approximation, the molecular field coefficient n can be determined from $k_B T_C = \mu_B n J_{sp}^0$. The second term reflects the influence of an external field and the third one approximates the anisotropy energy restricted (on the macroscopic level) to K_1 due to the elevated temperatures of interest here. The partition sum of an ensemble of magnetic moments can be written as [39]

$$Z = \sum_i \sum_{M_J=-\mathcal{J}}^{\mathcal{J}} \exp\left\{-\frac{1}{J_{sp}^0}\frac{\partial u}{\partial m_J}\frac{\mu_B \mu_0}{k_B T} g M_J\right\} \tag{21}$$

where M_J is the z-component of $\mathcal{J}$ of the i-th magnetic moment exposed to the exchange field of all other moments within the ensemble. With the free energy equal to $-k_B T \ln Z$ and eq.(20) it is found

$$m_J = B_J\left(\frac{3\mathcal{J}}{(\mathcal{J}+1)}\frac{T_C}{T} m_J + \frac{\mu_0 \mu_B g \mathcal{J}}{k_B T}\left[H\cos(\vartheta - \theta) - \frac{\sin^2\theta - \tfrac{2}{3}}{J_{sp}^0}\frac{\partial K_1}{\partial m_J}\right]\right) \tag{22}$$

where B_J is the Brillouin function and $J_{sp}^0 = \mu_0 \mu_B \rho g \mathcal{J}$. In the case of magnetic moments caused by spins only ($\mathcal{J} = \tfrac{1}{2}$, $g = 2$) eq.(22) simplifies to

$$m_J = \tanh\left(\frac{T_C}{T} m_J + \frac{\mu_0 \mu_B}{k_B T}\left[H\cos(\vartheta - \theta) - \frac{\sin^2\theta - \tfrac{2}{3}}{J_{sp}^0}\frac{\partial K_1}{\partial m_J}\right]\right) \tag{23}$$

The first term of the argument in eqs.(22) and (23) is well known from molecular field theory whereas the second and third term reflect the field and orientation dependency of J_{sp}, respectively. Note that eq.(23) can also be derived from minimizing F with respect to m_J (the entropy density for systems with $\mathcal{J} = \tfrac{1}{2}$ is given in [40]). Eq.(22) or (23) together with eq.(7) constitute a system of two coupled equations which can not be solved analytically. From eq.(22), the following implications on

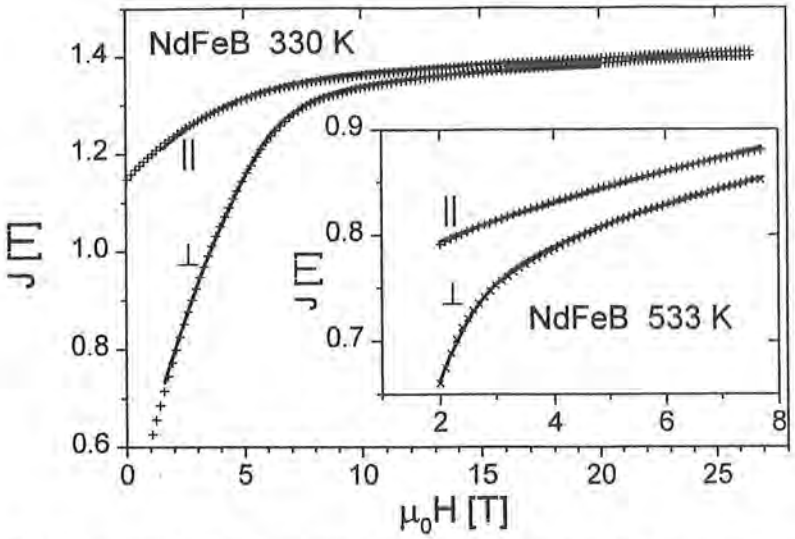

Fig.7: High field magnetization curves measured (markers) for a well textured NdFeB sample at 330 K. The field and orientation dependence of J_{sp} which is more pronounced at higher temperatures (inset: 533 K) was taken into account for the fitted curves (lines).

J_{sp} can be inferred: i) Within this approach, an perceptible field and orientation dependence of J_{sp} is only expected for temperatures close to T_C; it should be negligible at usual operating temperatures of permanent magnets. This may explain why we observed such effects for polycrystalline $Nd_2Fe_{14}B$ samples ($T_C \approx 584$ K) but not for $Sm_2Fe_{17}N_3$ up to temperatures of 533 K (approx. 0.7 T_C). ii) Both effects are more pronounced at higher values of g $\mathcal{J}$. iii) For observing the effects fields exceeding H_A are needed due to the field dependence of θ. iv) The orientation dependence of J_{sp} should only be present in materials of high MA. For a check of the introduced model, eq.(23) was incorporated into the fitting procedure and was solved simultaneously to the minimization of eq.(7), i.e. $J_{sp} = J_{sp}(T,H,\theta)$ was determined. With this, the DMC of NdFeB were fitted (examples are shown in Fig. 7) resulting in a maximum deviation of 3 mT between measured and calculated sample polarization values. It should be noted that the simplified assumption $\mathcal{J} = ½$, g = 2 is questionable for materials of uniaxial MA. The fit resulted in a value $J_{sp}^0 = 1.72$ T in agreement with measurements conducted at 4.2 K [41]. For NdFeB samples measured up to $0.9 \cdot T_C$, the ratio $\partial K_1/\partial m_J$ was estimated, $\partial K_1/\partial m_J \approx 3.8\ K_1/m_J$. Its experimental determination (results for K_1 and K_2 are presented in Fig. 1.b) and implications of this result on models describing MA will be discussed elsewhere [39]. For a more quantitative confirmation of the introduced model, however, DMC of single crystals will be analyzed.

5. Limitations of the introduced fit procedure

From a point of view of statistics, a proof of the basic question whether the model of reversible rotation of polarization of noninteracting grains is reliable for description of the demagnetization curves is given by the so-called χ^2-test [18]. From this, probabilities for the applicability of the model underlying the fit procedure are derived. As can be shown, the test is well fulfilled by the calculated demagnetization curves shown in Sect. 3.3. If the model is once established it can be used for an estimation of the accuracy of the fitted parameters. For the best textured NdFeB sample (cf. Sect. 3.3) it was found

$\Delta K_1 = \pm 0.4\ \mathrm{MJm^{-3}}$ $\quad$ $\Delta J_S = \pm 4\ \mathrm{mT}$

$\Delta K_2 = \pm 0.3\ \mathrm{MJm^{-3}}$ $\quad$ $\Delta \chi_p = \pm 6 \cdot 10^{-10}\ \mathrm{VsA^{-1}m^{-1}}$

$\Delta \sigma_g = \pm 1.0\ °$ $\quad$ $\Delta J_w = \pm 3\ \mathrm{mT}$,

where the sample dilution v is already taken into account. The given accuracies are mainly determined by the accuracies of the polarization measurements via eq.(8) and are typical values for the fit parameters shown in this paper (in case of the texture parameter its relative accuracy $\Delta\sigma_g/\sigma_g = 6\ \%$ has to be used). Investigation of the parameter correlation has shown that decreased values of χ_p and J_w increase the value of K_1 without any significant change of K_2. However, the values of the texture parameter σ_g and K_2 influence each other. It should be noted, that the given accuracies and correlations have been calculated on the basis of the reversible rotation of magnetization. Using the basic fit procedure (Sect. 3.1) six parameters can be determined with reasonable accuracy from the information provided by two independent DMC (measured parallel and perpendicular to the sample's texture axis). If either the number of parameters is increased without additional input information (as, e.g., given by the third independent DMC for non-rotationally symmetric texture function, Sect. 4.2) or the input information is reduced the fit results have to be considered with care as shown in the following examples: i) In case of an isotropic sample only one DMC provides significant information (cf. Sect. 3.3). Although the texture parameter is known for such a sample the reduced input information (one DMC only) is not completely compensated by the reduced number of parameters to be determined. In fact, χ_p and J_w can not be determined as accurate as given above resulting in higher inaccuracies of K_1. The latter may cause the slight deviation of H_A for the isotropic sample in Fig. 2. ii) For the sample $Dy_2Fe_{17}N_3$ a determination of K_3 was tried. It turned out, however, that the result for this additional parameter was strongly correlated to the result for K_2. Basically, these two parameters could not be resolved within reasonable limits of accuracy. iii) A phenomenological model [17] of two coupled sublattices has been considered to account for the different properties of the R and Fe sublattices in $Nd_2Fe_{14}B$. For this aim, eq.(7) was replaced by

$$F = K_1^R \sin^2\theta^R + K_2^R \sin^4\theta^R + K_1^{Fe} \sin^2\theta^{Fe} - \frac{n^*}{\mu_0} J_{sp}^R J_{sp}^{Fe} \cos(\theta^{Fe} - \theta^R) - H\left[J_{sp}^R \cos(\vartheta - \theta^R) + J_{sp}^{Fe} \cos(\vartheta - \theta^{Fe})\right] \tag{24}$$

Here, the superscripts correspond to the different sublattices and n^* is a coupling constant. The MA of the Fe sublattice can be well described [41] by only one anisotropy constant. To keep the number of parameters small $n^* = 268$ was assumed [42] and J_w omited (as possible for good NdFeB samples). The determined intrinsic parameters are: $K_1^R = 1.74\ \mathrm{MJm^{-3}}$, $K_2^R = 0.12\ \mathrm{MJm^{-3}}$, $J_{sp}^R = 0.28$ T, $K_1^{Fe} = 0.20\ \mathrm{MJm^{-3}}$, $J_{sp}^R = 1.0$ T. Although these results are in fair agreement with those given elsewhere [7], they show large correlations. Again, an increased number of fit parameters questions the reliability of the fit results. As indicated by the latter fact the main restriction for the fit procedure arises from the applicability of the model describing reversible rotation of $\vec{J}_{sp}$ of non-interacting, homogeneously magnetized grains, eqs. (7), (17) or (24). Smaller deviations from this assumption – due to, e.g., local fluctuations of the internal field or otherwise caused local inhomogeneities of the orientation of $\vec{J}_{sp}$ in a small part of the sample volume – may cause additional inaccuracies. If spatial regions in which deviations from a uniformly oriented J_{sp} have to be expected can not be neglected (as, e.g., in exchange coupled materials [43]) the interpretation of the fit results becomes difficult or even impossible. As already mentioned (cf. Sect. 3.3) the texture function itself can not be determined by the fit procedure. An appropriate function must be known from either the

sample fabrication process or complementary investigations (e.g. X-ray). More detailed results could be expected if DMC were measured and analyzed for additional sample orientations τ in between the parallel and perpendicular ones, $0 \leq \tau \leq \pi/2$.

6. Summary

Fitting of demagnetization curves was utilized to determine the anisotropy constants K_1 and K_2 of magnetically uniaxial material, its spontaneous polarization J_{sp} and a texture parameter of polycrystalline samples. The applicability of the method was proven by investigating NdFeB materials for which the intrinsic parameters are known from single crystal measurements, by checking the consistency of the results using differently textured samples as well as by statistics. Thereafter, the established method was applied to R-T-materials the anisotropy field of which can be much higher than the maximum measuring field. These results were used to gain more insight into the CEF of those materials. Materials of different types of MA were investigated: easy axis, easy plane and, after adapting the basic fit procedure, non-uniaxial MA in 3:29 compounds. In addition, materials of biaxial texture were investigated and comparative X-ray measurements showed the reliability of the procedure. Results on J_{sp} were discussed in the framework of a thermodynamical model which takes into account the field and orientation dependence of J_{sp}. Since the introduced fit procedure relies on reversible rotational processes of J_{sp} the application of the fit are also limited by these processes.

Acknowledgment

The author is especially grateful to A. Handstein, D. Hinz and A. Margarian for preparation of the various samples. The pole figure measurement by D. Schläfer are acknowledged. For fruitful discussions I am indebted to D. Eckert, M. Wolf, K.-H. Müller, J. M. D. Coey and S. von Molnár. The work was partially supported by the *Alexander von Humboldt-Foundation*, Germany.

References

[1] *Handbook of Magnetic Materials*, ed. E. P. Wohlfarth (vol. 1-3), eds. E. P. Wohlfarth and K. H. J. Buschow (vol.4), ed. K. H. J. Buschow (vol. 5-10), North-Holland, Amsterdam 1980-1997.
[2] K. H. J. Buschow in [1], vol. 4, p.1.
[3] I. A. Campbell, *J. Phys.* F 2 (1972) L47.
[4] W. F. Brown, *Rev. Mod. Phys.* 17 (1945) 15.
[5] W. Döring, in *Handbuch der Physik, Band XVIII/2*, ed. H. P. J. de Wijn, Springer, Berlin 1966, p.341.
[6] T. Holstein and H. Primakoff, *Phys. Rev.* 58 (1940) 1098.
[7] J. J. M. Franse and R. J. Radwanski, in [1], vol. 7, p.307.
[8] E. R. Callen and H. B. Callen, *J. Phys. Chem. Sol.* 16 (1960) 310.
[9] J. M. Alameda, D. Givord, R. Lemaire and Q. Lu, *J. Appl. Phys.* 52 (1981) 2079.
[10] K. H. J. Buschow in [1], vol. 1, p.297.
[11] M. T. Hutchings, in *Solid State Physics*, Vol. 16, ed. F. Seitz and D. Turnbull, Academic Press New York, 1964, p.227.

[12] J. Smit and H. P. J. Wijn, *Ferrite*, Philips Technische Bibliothek, Centrex, Eindhoven 1962, p.50
[13] G. Asti and S. Rinaldi, *J. Appl. Phys.* 45 (1974) 3600.
[14] M. Katter, J. Wecker, C. Kurth, L. Schultz and R. Grössinger, *J. Magn. Magn. Mater.* 117 (1992) 419.
[15] K.-H. Müller, D. Eckert, P.A.P. Wendhausen, A. Handstein, S. Wirth, M. Wolf, *IEEE Trans. Magn.* 30 (1994) 586.
[16] E. C. Stoner and E. P. Wohlfarth, *Phil. Trans. Roy. Soc.* 240 (1948) 599.
[17] G. Asti, in [1], vol. 5, p.396.
[18] I. N. Bronstein and K. A. Semendjajew, in *Handbook of Mathematics*, Teubner Verlag Leipzig, 1985, p.689 (german).
[19] D. Givord, A. Lienard, R. Perrier de la Bathie, P. Tenaud and T. Viadieu, *J. Phys. Colloq.* 46 (1985) C6-313.
[20] H. Kronmüller, K.-D. Durst and G. Martinek, *J. Magn. Magn. Mater.* 69 (1987) 149
[21] G. Asti, F. Bolzoni and L. Pareti, *J. Magn. Magn. Mater.* 83 (1990) 270.
[22] L. Jahn, K. Elk and R. Schumann, *J. Magn. Magn. Mater.* 68 (1987) 335.
[23] G. Asti, R. Cabassi, F. Bolzoni, S. Wirth, D. Eckert, P. A. P. Wendhausen and K.-H. Müller, *J. Appl. Phys.* 76 (1994) 6268.
[24] S. Wirth, R. Skomski and J. M. D. Coey, *Phys. Rev. B* 55 (1997) 5700.
[25] S. Wirth, M. Wolf, K.-H. Müller, R. Skomski, S. Brennan and J. M. D. Coey, *IEEE Trans. Magn.* 32 (1996) 4746.
[26] J. M. D. Coey, Hong Sun and Y. Otani, Proc. *6th Int. Symp. on Magnetic Anisotropy and Coercivity in RE-TM Alloys*, Pittsburgh 1990, p.36.
[27] J. M. D. Coey and H. Sun, *J. Magn. Magn. Mater.* 87 (1990) L251.
[28] H.-S. Li and J. M. Cadogan, *Solid State Comm.* 80 (1991) 905.
[29] H. Kato, M. Yamada, G. Kido and Y. Nakagawa, *J. Appl. Phys.* 73 (1993) 6931.
[30] M. D. Kuz'min, *Phys. Rev. B* 46 (1992) 8219.
[31] T. S. Zhao, X. C. Kou, R. Grössinger and H. R. Kirchmayr, *Phys. Rev. B* 44 (1991) 2846.
[32] R. Coehoorn and G. H. O. Daalderop, *J. Magn. Magn. Mater.* 104-107 (1992) 1081.
[33] J. M. Cadogan, H.-S. Li, A. Margarian, J. B. Dunlop, D. H. Ryan, S. J. Collocott and R. L. Davis, *J. Appl. Phys.* 76 (1994) 6138.
[34] O. Kalogirou, V. Psycharis, L. Saettas, D. Niarchos, *J. Magn. Magn. Mater.* 146 (1995) 335.
[35] S. Wirth, M. Wolf, A. Margarian and K.-H. Müller, *9th Int. Symp. on Magnetic Anisotropy and Coercivity in RE-TM Alloys*, Sao Paulo 1996, p.399.
[36] D. Hinz, S. Wirth, D. Eckert, K. Helming, K.-H. Müller, *J. Magn. Magn. Mater.* 157/158 (1996) 43.
[37] T. Shimoda, K. Akioka, O. Kobayashi, T. Yamagami and A. Arai, *11th Int. Workshop on RE Magnets and their Applications*, Pittsburg 1990, p.17.
[38] S. Hock, Thesis, MPI für Metallforschung Stuttgart, Germany, 1988.
[39] S. Wirth, M. Wolf and K.-H. Müller, to be published.
[40] S. V. Vonsovskii, *Magnetism*, Nauka, Moscow, 1971 (russ.).
[41] J. M. Cadogan, J. P. Gavigan, D. Givord and H. S. Li, *J. Phys. F* 18 (1988) 779.
[42] N. H. Duc, T. D. Hien, D. Givord, J. J. M. Franse and F. R. de Boer, *J. Magn. Magn. Mater.* 124 (1993) 305.
[43] K.-H. Müller, D. Eckert, A. Handstein, M. Wolf, S. Wirth, L. M. Martinez, *8th Int. Symp. on Magnetic Anisotropy and Coercivity in RE-TM Alloys*, Birmingham 1994, p.179.